JOURNAL OF ENERGY SYSTEMS

2022, 6(3)

2602-2052 DOI: 10.30521/jes.1055935 Research Article

Theoretical and computational studies on the optimal positions of NACA airfoils used in horizontal axis wind turbine blades

Getahun Tefera
University of KwaZulu-Natal, Mechanical Engineering Department, Durban, South Africa, getmechanical@gmail.com
Glen Bright
University of KwaZulu-Natal, Mechanical Engineering Department, Durban, South Africa, brightg@ukzn.ac.za
Sarp Adali
University of KwaZulu-Natal, Mechanical Engineering Department, Durban, South Africa, adali@ukzn.ac.za

Submitted: 10.01.2022
Accepted: 15.08.2022
Published: 30.09.2022

Abstract: This paper presents a theoretical and computational study to determine the optimal positions of airfoils along the length of the horizontal axis wind turbine blade. We used four and five-digit NACA airfoils to model a 54-meter blade. The lift, drag coefficient, and lift-to-drag ratio of each airfoil are determined by using QBlade software. The aerodynamic performance of the airfoils is studied based on the blade element momentum theory, and Matlab software is used for numerical implementation. The velocity and pressure distributions on each airfoil are assessed using computational fluid dynamics. We implement the thickness distribution techniques to adjust the positions of the airfoils along the length of the blade. It is noted that stresses reach their maximum values at the root and minimum at the tip section. Thus, the thicker (NACA 4420) and thinner (NACA 23012) airfoils are set at 20% of the maximum chord and 91.11% at the tip sections of the blades. The remaining sections of the blade are configured using linear interpolation methods. Specifically, the maximum chord length of the new design is reduced by 18.06% compared to the NACA 23012 rotor blade. Finally, the recommended tip speed ratio for the designed rotor blade is estimated using the graphs of the normal and tangential forces, thereby producing a safe and efficient design.

Keywords: *Aerodynamic performance, Blade element momentum theory, Computational fluid dynamics, NACA airfoils, Wind energy*

Cite this paper as: Tefera, G., Bright, G., & Adali, S., Theoretical and computational studies on the optimal positions of NACA airfoils used in horizontal axis wind turbine blades. *Journal of Energy Systems* 2022; *6*(3): 369-386, DOI: 10.30521/jes.1055935.

Nomenclature

HAWT	Horizontal Axis Wind Turbine	V_1	Wind velocity
α	Angle of Attack (AOA)	c	Airfoil chord
φ	Angle of relative wind	θ_T	Section twist angle
NACA	National Advisory Committee for Aeronautics	U_{rel}	Relative wind speed
BEM	Blade Element Momentum Theory	r	Rotor radius
CFD	Computational Fluid Dynamics	λ	Tip speed ratio
NREL	National Renewable Energy Laboratory	λ_r	Local speed ratio
DU	Delft University	ω	Angular velocity
R	Blade length, Rotor Radius	ρ	Air Density
N	Number of Blade Element	ν	Kinematic Viscosity
B	Blade Number	μ	Air Viscosity
Re	Reynolds Number	C_D	Drag coefficient
L	Lift Force	C_L	Life coefficient
D	Drag Force	FN	Normal force
F	Tip loss factor	FT	Tangential force
f	Tip loss factor coefficient	dr	Section radius distance
Cx	Axial force coefficient	Cp	Power coefficient
Cy	Tangential force coefficient	σ'	Solidity factor
P	Power output		

1. INTRODUCTION

Renewable energy generation systems have been important resources in current energy production for some decades world-widely. Clean, efficient, low-cost, and long term energy sources are the primary solutions to the world's ever increasing energy demand and over dependency on fossil fuels [1]. Wind energy is one of the renewable energy sources with a relatively low cost as compared to other sources of green energy and with minor environmental effects. Nevertheless, the latest geopolitical events have put a spotlight on the urgent need to reinforce the security of supply, reduce fossil fuel energy dependency, and shield against market disruption caused by high prices [2,3]. Again, this can be achieved with a massive deployment of renewables. European countries, in particular, have set a goal of increasing their gross energy consumption from renewable energy sources to 32% by 2030. According to European wind energy statistics, 17.4 GW of new wind power capacity was installed in 2021. The wind energy capacity of the countries reached 236 GW [4]. The amount of power that can be harvested from wind depends on the size of the turbine and the length of its blades. The output is proportional to the dimensions of the rotor and the cube of the wind speed.

Wind turbine blades perform the most important function in the wind energy conversion system that harvests the wind and converts the kinetic energy of the airflow into rotational mechanical energy, which is then transformed into electrical energy by a generator. Choosing an effective blade geometry is a key element for extracting the maximum kinetic energy from the wind [5,6]. The shape of the blade and velocity of the wind has an effect to obtain the maximum possible power output. In particular, the geometry of the blade profiles has a direct effect on improving the aerodynamic efficiency [7]. Selecting an optimal shape is the most important and complex process. However, experimental and numerical studies have continued to optimize the profile of airfoils to optimize their efficiency [8,9,10]. Improving the shape of the rotor involves both aerodynamic and structural issues [11]. Aerodynamic optimization of the rotor is achieved through the proper choice of airfoil shape, tip speed ratio, number of blades, distribution of chord length, and angle of the relative wind. In particular, the aerodynamic efficiency at the tip section of the rotor should be as high as possible to maximize the power coefficient. Meanwhile, higher stress could occur in the root section. Increasing the thickness and the chordwise length of the airfoil is a technique for improving blade strength and stiffness [12].

The airflow around the surface of the airfoil causes lift and drag forces due to the pressure variations between its upper and lower surfaces. To maximize the power coefficient, the lift coefficient and lift-to-drag ratio of the airfoils must be higher. While the drag coefficient of the airfoils must be lower [13]. The effect of different angles of attack on the values of lift and drag forces by considering the NACA 4420 airfoil was investigated in [14]. An important objective is to find the optimum distribution of the airfoil and pitch angle considering design parameters such as relative wind speed, angle of attack, and tip speed ratio (TSR). Selecting the proper TSR is the fundamental parameter in the design of a horizontal axis wind turbine (HAWT) blade to extract more energy from the wind [15,16].

Blade element momentum theory (BEMT) is the basic theoretical method used by researchers and manufacturers to predict the performance of HAWT blades. BEMT is a combination of momentum theory and blade element theory. It is an iterative process to compute the relative wind velocity induced at the rotor, axial, and tangential induction factors to determine the chord length with a defined TSR [17]. The model divides the blade into several sections from the root to the tip of the blade to determine the aerodynamic forces on each element. These forces can be calculated as a two-dimensional airfoil subjected to the flow conditions. Testing the performance of airfoils using a wind tunnel is often time-consuming and leads to higher costs. Indeed, wind turbine blade designers frequently use theoretical studies to optimize the aerodynamic performance of the airfoils. Numerical studies can save time and material costs compared to experimental studies. The aerodynamic performance of a small and 5 kW of the HAWT blade was studied using BEMT in [18] and [19] to assess the optimum twist angle and chord

length [18]. Additionally, the geometry of the blade was developed using two NACA airfoils in [20] and the aerodynamic performance was investigated using BEMT to determine the chord, thickness, and twist distributions [21]. Additionally, Mujahid et al. [22] compared the power output of four different wind turbine blades with eight different NACA airfoils using BEMT and Q-Blade simulation code. Each blade was constructed as a combination of NACA airfoils oriented along its length and simulated at different Reynolds numbers. They determined the maximum power coefficient by varying the chord length, twist angle, and lift coefficient. The power coefficient of different airfoil families needs to be assessed before developing the blade. Padmanabhan and Saravanan [23] compared the power coefficients of two blades developed using NREL and NACA airfoils based on the same wind speed. They found that maximum power extraction for the NACA blade was at around 10 m/s and for the NREL blade was within a range of 3 to 9 m/s. The results showed that NREL airfoil extracts the maximum power at lower wind speed than NACA airfoil. These results show the advantages of developing the geometry of the blade using different airfoil families to maximize the power coefficient.

Nowadays, using computer-aided design codes, the aerodynamic performance of HAWT blades can be assessed by using computational fluid dynamics (CFD) software [24,25]. Han Cao used [26] CFD software to study the aerodynamic performance of a HAWT blade. The geometry of a HAWT blade was developed using DU-93 and NREL-S809 airfoils. The results indicated the variations in the aerodynamic performances of the airfoils. In addition to 2D models, 3D models were also used to study the performance of a small-sized HAWT blade. Additionally, Carlo Carcangiu [27] investigated the physical behaviour of the flow field past the blades, around the boundary layer and in the wake regions. The full wind turbine blade model was investigated with the help of the 3D Navier–Stokes solver ANSYS Fluent software. The rotational effect on the boundary layer of the blade was investigated to obtain a complete solution database and a post-processing tool**.**

Nowadays, different types of airfoil families have been used to produce HAWT blades. The airfoils were selected based on their aerodynamic performance under variable wind loads. Due to the wind forces, the maximum stress occurs at the root sections, and the minimum stress is at the tip sections. A thicker airfoil is needed for higher stress areas and a thinner airfoil for lower stress areas, respectively. With the background knowledge described above, it is clear that the efficiency of the blade is primarily dependent on the performance of each airfoil along the length of the blade. The performance of four- and five-digit airfoils can have different performances. Developing the blades using four and five-digit airfoils is one technique to maximize the aerodynamic performance. However, it is necessary to carry out further investigations into it.

In the present work, the performance of four and five-digit NACA airfoils such as NACA 4415, NACA 4420, NACA 23012, and NACA 23015 airfoils was selected to set optimized locations for designing 54 m HWAT blades. We used thickness distribution techniques to assess optimal locations. The aerodynamic performance of the airfoils was characterized using CFD, BEMT, and Q-blade simulation codes. Maximum structural stability, lower weights, reduced flow in the spanwise direction, and shorter chord lengths were obtained when hybrid NACA 4420, NACA 23015, NACA 4415, and NACA 23012 airfoils were used on hybrid HAWT at 20%, 37.78%, 55.56%, and 91.11% of the full length. A circular profile was used to cover the remaining parts of the blade, from the maximum chord to the root section of the blade.

2. METHODOLOGY

In the present study, four airfoil geometries, namely, NACA 4415, NACA 4420, NACA 23015, and NACA 23012 are selected to positions along the blade length of $R = 54\,m$. The number of blade elements is set to $N = 10$ and the number of blades is specified as $B = 3$. The aerodynamic performance of airfoils is characterized by using non-dimensional parameters (Re) under different angles of attack (AOA). The shape of the airfoil for the HAWT blades should have a high lift coefficient, a low drag

coefficient, roughness in the leading edge, and good stall performance to optimize the aerodynamic performance and be assessed by different authors [28], [29]. Airfoil characteristics, including L/D, C_L, and C_D are estimated by Q-Blade/ XFoil simulation software. The Q-Blade/XFoil software is open-source and is used to study the performance of NACA airfoils at different Re and AOA. The optimal geometry depends on the cross-sectional shape of the blade. The width and twist angles of each airfoil are defined by using BEMT to achieve the maximum power coefficient. With good reliability and rapid evaluation, BEMT is recommended by different researchers for use for optimization of the performance of the blade [22]. The Reynolds numbers of large wind turbine blades mostly vary between 1×10^6 and $1 \times 10^7$for the range of 200kW–6MW HAWTs. We used five Reynolds numbers, namely, 2×10^6, 4×10^6, 6×10^6, 8×10^6, and 1×10^7 for a range of AOA between 0^o and 25^o. Re is given by:

$$Re = \frac{V_1 c}{\nu} = \frac{\rho V_1 c}{\mu} = \frac{Inertial\ force}{Viscous\ force} \quad (1)$$

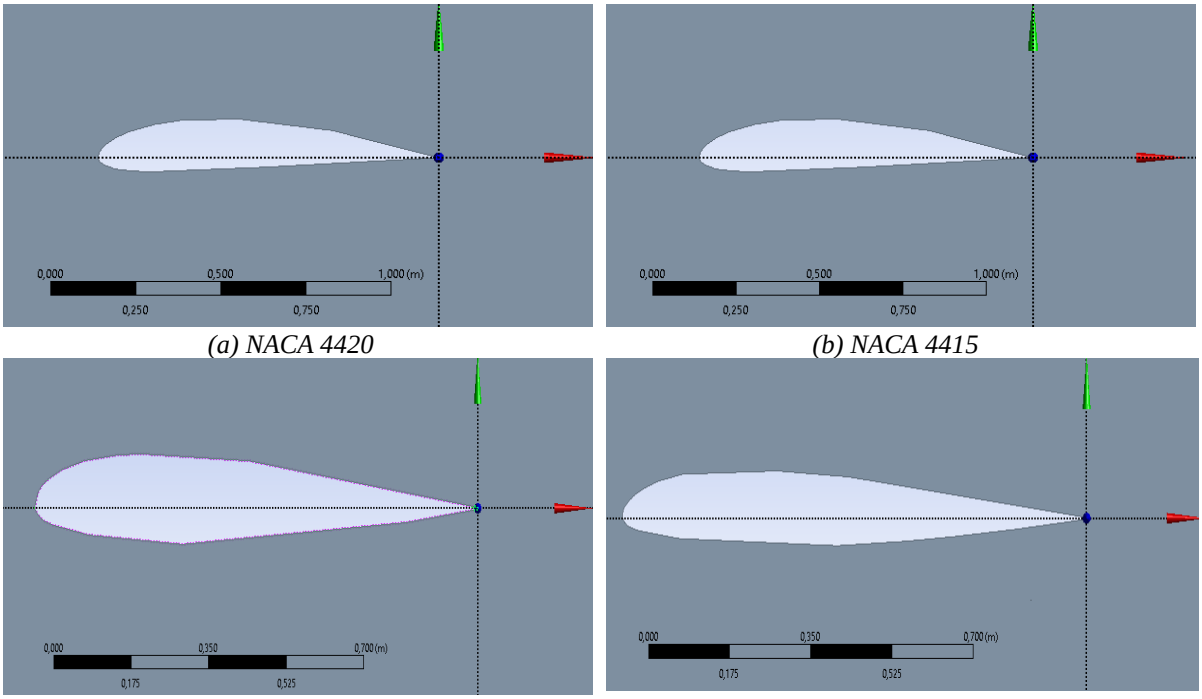

(a) NACA 4420 *(b) NACA 4415*

(c) NACA 23015 *(d) NACA 23012*

Figure 1. The geometry of NACA 4 and 5-digit airfoil geometry.

3. BLADE DESIGN OPTIMIZATION

3.1. Tip-Speed Ratio (TSR)

TSR is the ratio of rotor speed to wind speed, which is related to the power coefficient. A blade that rotates slowly due to an inefficient design of the rotor allows the wind to pass through and extracts a relatively low amount of energy (low TSR). However, if the wind blades rotate at a high speed (high TSR), the blades act like a solid wall to the incoming wind. The optimal energy cannot be extracted in this situation as it may cause the blade to be highly stressed, increasing the possibility of structural failure. Designing the rotor with an optimal TSR is necessary to extract the maximum power from the wind with an improved lifetime of the rotor. The optimum TSR depends on the number of blades used to produce the wind turbine. The majority of wind farms around the world use two to four-bladed rotors with an optimized TSR of 5 to 6. The TSR can be increased by using highly efficient airfoils in the design and modelling of the rotor. A proper design of a three-bladed rotor would have a TSR ranging

between six and eight [15]. In the present study, 7, 8 and 9 tip speed ratios are considered for 54 m HAWTs. The relationship between the free stream wind speed and the angular velocity of wind at the rotor is considered by the non-dimensional factor, λ given by:

$$Tip\ speed\ ratio: \lambda = \frac{speed\ of\ rotor\ tip}{Wind\ speed} = \frac{v}{V_1} = \frac{\omega r}{V_1} \quad (2)$$

Higher TSR results in a higher rotational speed of the shaft, leading the generator to operate at a high level of efficiency. However, the erosion of the leading edges, higher noise levels, and vibration of the turbine are the disadvantages of a high tip speed ratio. The local speed ratio λ_r, is given by

$$\lambda_r = \frac{\lambda r}{R} \quad (3)$$

3.2. Twist and Chord Distribution

The maximum energy can be extracted when the shape of the blade has been constructed from an optimized chord and twist angle along the length of the HAWT blades. Based on BEMT, different formulas have been developed to optimize the basic parameters (chord length and twist angle) of the airfoils [15]. It is needed to optimize these parameters based on TSR along the length of the blade. Thus, the lift coefficient at the most efficient AOA of the airfoil is given by

$$c(r) = \frac{1}{B}\frac{16\pi r}{C_L} sin^2\ (1/3\ arctan(\ R/\lambda r)) \quad (4)$$

The angle between the relative wind velocity and the plane of rotation can be obtained from

$$\varphi(r) = 2/3\ arctan(\ R/\lambda r) \quad (5)$$

Considering the blade pitch angle constant, the section twist angle can be estimated by:

$$\theta_T(r) = \varphi(r) - \alpha \quad (6)$$

The AOA α, and the maximum C_L values of NACA 4415, NACA 4420, NACA 23012, and NACA 23015 each airfoil are computed using Q-blade simulation code.

3.3. Blade Element Momentum Theory (BEMT)

BEMT is a combination of blade element theory and momentum theory. The blade element theory is used to assess the forces acting on each section of the blade due to airflow. In momentum theory, free stream air velocity is assumed to be a flow tube and is used to estimate the ideal efficiencies and flow velocities, which involve estimating the forces acting on the wind rotor. The combined theory is used to achieve the optimal blade shape, leading to improved rotor performance. The parameters involved in the computations include flow angle, AOA, induction factors, chord length, tip loss factor, solidity rate, and different forces used to maximize the power coefficients.

The flow angle φ between each section based on the axial induction factor$(a)$and the angular induction factor (a') can be computed from

$$\varphi = tan^{-1}\left(\frac{(1-a)V_1}{(1+a')\omega r}\right) \quad (7)$$

Values of a' developed by using the Betz limit [30] which is one of the parameters to model the geometry of a blade. The angular and axial induction factors are set initially to zero and $1/3$, respectively, to estimate the flow angle. The axial induction factor (a)is determined from

$$a = \frac{1}{[1 + 4F\,sin^2\,\varphi\,/(\sigma' C_L\,cos\,\varphi)]} \tag{8}$$

The tip loss factor (F) is estimated from

$$F = \frac{2}{\pi} cos^{-1}(e^{-f}) \tag{9}$$

The value of f is calculated from

$$f = \frac{B}{2}\frac{R - r}{r - sin\,\varphi} \tag{10}$$

σ' is the solidity factor which is determined from

$$\sigma' = \frac{cB}{2\pi r} \tag{11}$$

The axial force coefficientC_x is obtained from

$$C_x = C_L\,cos\,\varphi + C_D\,sin\,\varphi \tag{12}$$

The angular induction factor(a') based on BEM theory can be determined from

$$a' = \frac{1}{[(4F\,cos\,\varphi\,/(\sigma' C_L)) - 1]} \tag{13}$$

The tangential force coefficientC_y is obtained from

$$C_y = C_L\,sin\,\varphi - C_D\,cos\,\varphi \tag{14}$$

The values of$a$anda' computed from equations (8) and (13) are used as the initial values for the flow angle iteration given by equation (7). The stopping criteria for the iteration process are given by

$$|a_{n+1} - a_n| < 0.001 \text{ and} |a'_{n+1} - a'_n| < 0.001$$

Once the values of$a$ and a' converge, the relative wind speed for the given flow angle is determined from

$$U_{rel} = \frac{V_1(1 - a)}{sin\,\varphi} \tag{15}$$

Considering *B* blades, the axial force in a section at a distance$r$ (i.e., relative wind velocity, axial and tangential forces on each section) can be calculated from

$$dF_N = B\frac{1}{2}\rho U_{rel}^2(C_L\,cos\,\varphi + C_D\,sin\,\varphi)cdr \tag{16}$$

The tangential force in each section of the blade can be computed from

$$dF_T = B\frac{1}{2}\rho U_{rel}^2(C_L \sin\varphi - C_D \cos\varphi)cdr \quad (17)$$

The torque on the section is obtained from

$$dT = B\frac{1}{2}\rho U_{rel}^2(C_L \sin\varphi - C_D \cos\varphi)crdr \quad (18)$$

The power generated by the blade element can be calculated from

$$dP = dT\omega \quad (19)$$

The non-dimensional power coefficient based on the axial induction factors is determined from

$$C_P = \frac{\frac{1}{2}\rho A V_1^3 4a(1-a)^2}{\frac{1}{2}\rho A V_1^3} = 4a(1-a)^2 \quad (20)$$

The power output of a wind turbine blade can be expressed as

$$P_{out} = \frac{1}{2}\rho A V_1^3(\eta_{Mech} C_P) \quad (21)$$

3.4. Computational Fluid Dynamics (CFD) Method

The aerodynamic performance of the airfoil can be predicated on using CFD software. The two-equation shear stress transport (SST) $k-\omega$, Reynolds Averaged Navier Stokes (RANS), and Spalart-Allmaras turbulence models are the known solution methods in the ANSYS Fluent software [31]. The SST $k-\omega$ model is more accurate in predicting the area of flow separation caused by the adverse pressure gradients as noted in Refs. [15] and [19]. In this study, the SST $k-\omega$ model is considered to perform numerical simulations on the specified airfoils. Three operational wind speeds, such as 6, 9, and 12 m/s, and a designed angle of attack $\alpha_D = 9^0$ are considered to predict the values of turbulence kinetics, velocity, and pressure distribution on each airfoil.

The coordinates of each airfoil are computed using the airfoil database and imported into the ANSYS design modeler to create 2D geometries. The chord length with a length of 1 m on each airfoil is specified. The C-mesh type for the flow field geometry and boundary conditions are set around the airfoil as shown in Fig. 2. The length and width of the C-mesh for the grid cells are set at 25 times the chord length. The input and output layers of the boundary locations are represented by curve A and line G. The tip of the airfoil curves is located at point D. The symmetrical parts of the wall are the edges BE and CF. The geometry of boundary layers is divided by structured quadrilateral cells to form a mesh as shown in Fig. 3. The meshing overview and boundary conditions for simulations for each airfoil are given in Tables 1 and 4. The cell of the layers can be considered as a very small volume in which the conservation equations can be solved. The quadrilateral meshes consist of approximately 40000, 49000, and 246000 cells. The meshed geometry is imported to ANSYS Fluent to determine the problem parameters and run the CFD simulations [32].

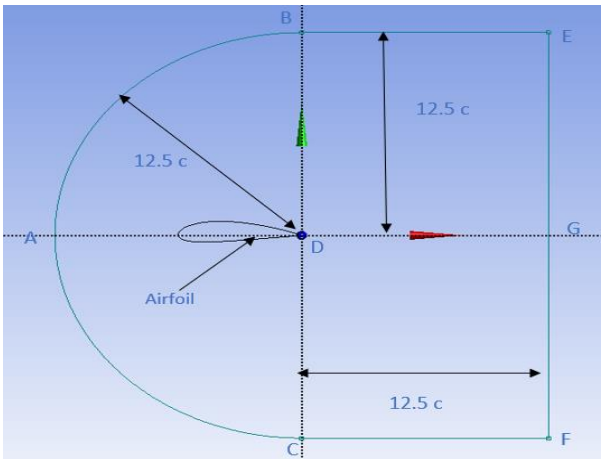

Figure 2. C-mesh type flow domain and the boundary conditions.

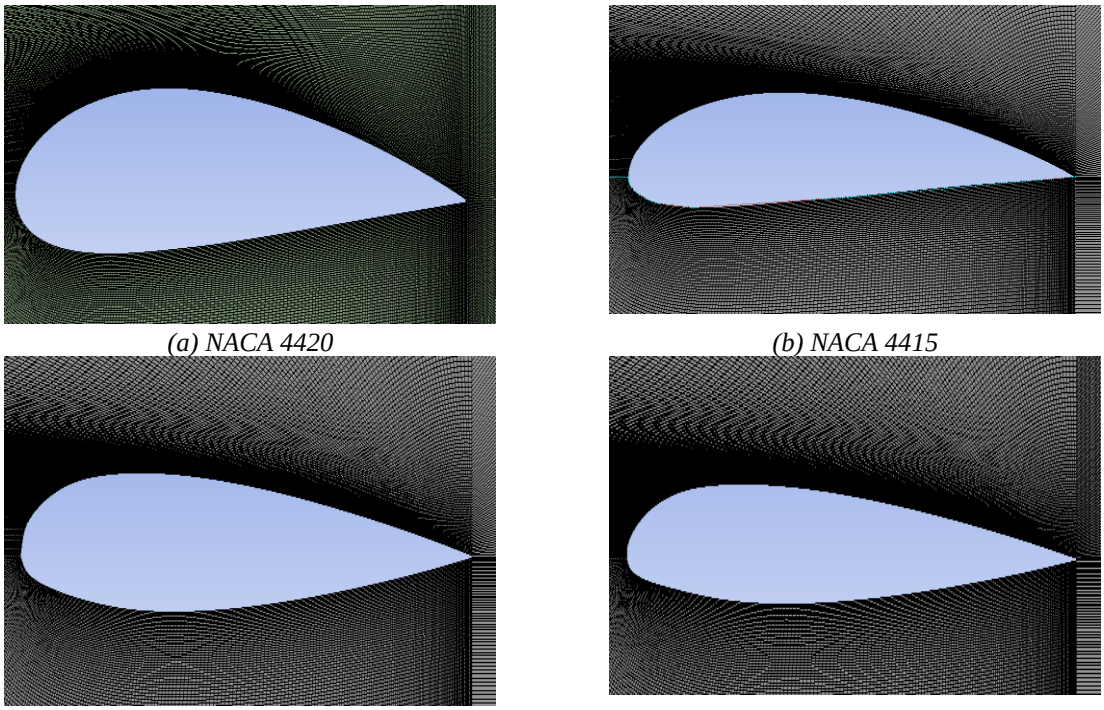

(a) NACA 4420 *(b) NACA 4415*

(c) NACA 23015 *(d) NACA 23012*

Figure 3. Meshed flow domain and the boundary layers.

Table 1. Boundary conditions for CFD simulations.

Simulation type	Pressure based steady simulation
Fluid material and flow type	Air, incompressible flow
Temperature	288.16 K
Density of air	1.225 Kg/m^3
Kinematic viscosity	1.48 x 10^{-5} m^2/s
Pressure	101 325 Pa
Wind speeds	6, 9, 12 m/s
Angle of attack	$\alpha_D = 9^0$
Turbulence model	SST $k-\omega$
Solution method	Pressure-velocity coupling, Least square cell-based, Second-order- pressure, Second-order upwind-momentum, Second-order upwind- turbulence, Second-order upwind-specific energy dissipation rate
Solution control	Pressure: 0.5 Momentum: 0.5 Turbulent kinetic energy: 0.75
Boundary conditions	Velocity inlet (6, 9, 12m/s), Pressure outlet (gauge pressure): 0
Number of mesh cells	40000, 89000 and 246000

4. RESULTS AND DISCUSSIONS

4.1. Airfoil Properties

The shape of the airfoil can be capable of generating significantly more lift force than drag force. It is necessary to know the relationship between the lift, drag coefficient, and angle of attack of the airfoils at different Reynolds numbers before developing the blades [33]. Figs. 4 (a-e) shows the values of lift and drag coefficients of four NACA airfoils as a function of an angle of attack (α) under different Reynolds numbers (*Re*). As observed in the curves, the values of lift coefficients of NACA 4415, NACA 4420, NACA 23012, and NACA 23015 are increasing as the Reynolds numbers are increasing. However, these changes in lift coefficients of the targeted airfoils occur up to about $\alpha = 17^{o}$ and then start decreasing after reaching their maximum values. Additionally, the maximum values of lift coefficients, drag coefficients, and lift-to-drag ratios of the targeted NACA airfoils, considering different Reynolds numbers, are shown in Table 2. It is indicated that the lift and drag coefficient of the NACA 4415 airfoil is the highest value as compared to other airfoils under consideration. However, the lift-to-drag ratio of the NACA 4415 airfoil is the lowest value at$Re = 6 \times 10^{6}$, respectively.

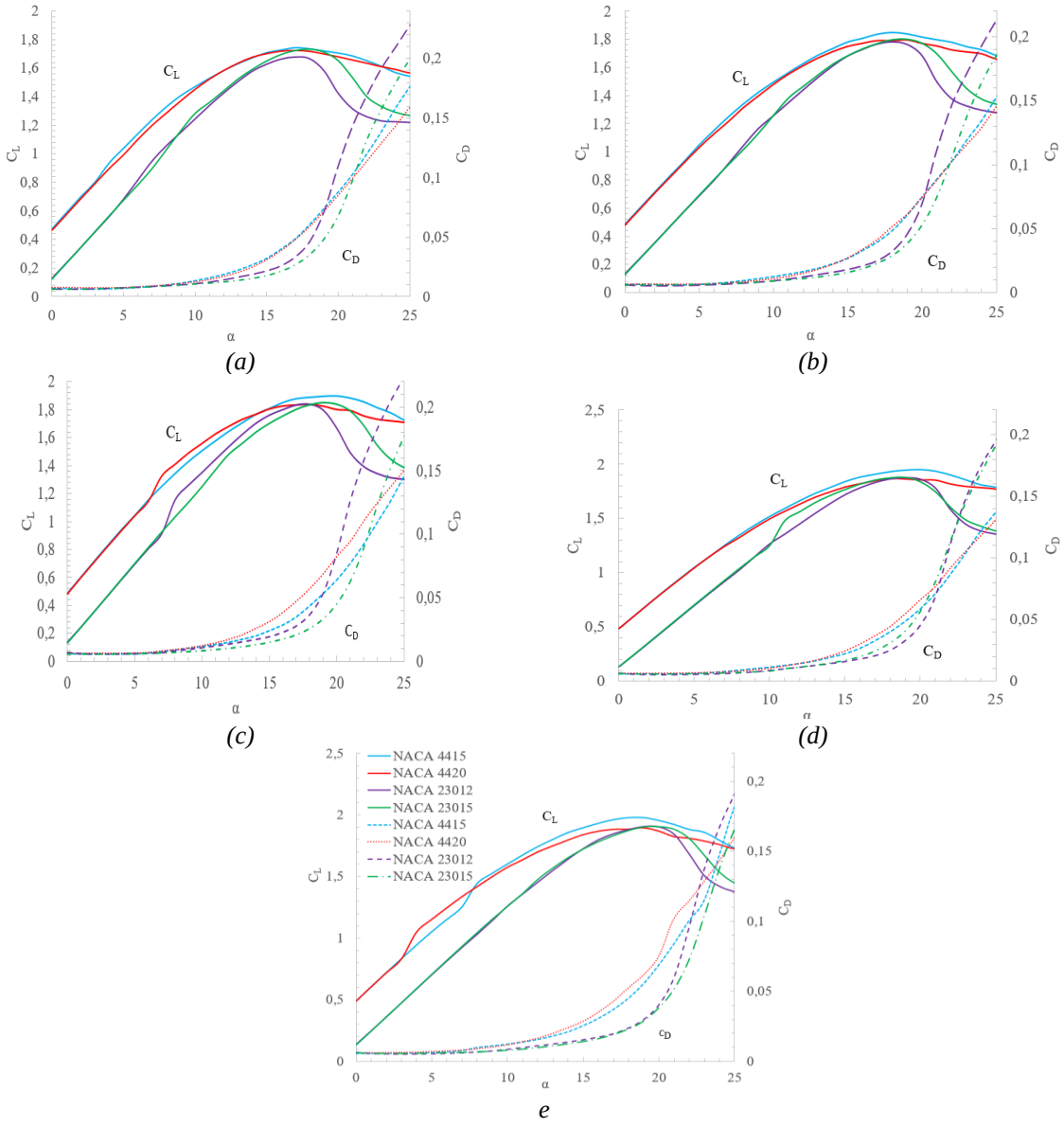

Figure 4. Lift and drag coefficient of airfoils at a different angle of attacks and Reynolds number (a) $Re = 2 \times 10^{6}$, (b) $Re = 4 \times 10^{6}$, (c) $Re = 6 \times 10^{6}$, (d) $Re = 8 \times 10^{6}$, and (e) $Re = 1 \times 10^{7}$.

Table 2. Maximum values of drag and lift coefficients and lift-to-drag ratios for $2E6 \leq Re \leq 1E7$.

Airfoils	NACA 4415			NACA 4420			NACA 23012			NACA 23015		
Parameters	Cd	Cl	Cl/Cd	Cd	Cl	Cl/Cd	Cd	Cl	Cl/Cd	Cd	Cl	Cl/Cd
Re: 2E6	0.048	1.743	36.313	0.048	1.722	35.875	0.046	1.665	36.196	0.035	1.730	49.429
Re: 4E6	0.048	1.846	38.458	0.062	1.794	28.935	0.033	1.779	53.909	0.038	1.802	47.421
Re: 6E6	0.064	1.900	29.688	0.057	1.837	32.228	0.037	1.839	49.703	0.034	1.849	54.382
Re: 8E6	0.059	1.949	33.034	0.055	1.864	33.891	0.033	1.874	56.788	0.041	1.882	45.902
Re: 1E7	0.055	1.978	35.964	0.062	1.897	30.597	0.030	1.908	63.600	0.038	1.905	50.132

The primary function of the airfoil is to increase lift force by reducing the pressure on the upper surface of the airfoil. It is important to select an airfoil shape that will give a high lift and lift-to-drag ratio at different Reynolds numbers. In particular, the high lift-to-drag ratio of an airfoil is desirable for small-sized rotors to generate optimum power at low wind speeds [13]. The relationship between the power coefficient and the lift-to-drag ratio of an airfoil is studied in [34]. The maximum power coefficient can be obtained by increasing the L/D of the airfoils of the blade. Therefore, maximizing the lift-to-drag ratio of the airfoils can support getting the optimal power coefficient. In this study, the lift-to-drag ratio of four airfoils is characterized by considering different AOA and Re on NACA 4415, NACA 4420, NACA 23012, and NACA 23015 airfoils as shown in Fig. 5 (a-e). As the AOA increases, the lift-to-drag ratios of all airfoils reach their maximum values and then decrease drastically. The lift-to-drag ratio of four NACA airfoil families is compared by considering the Reynolds numbers of $Re = 2 \times 10^6$ as shown in Fig. 5(a). Considering NACA 4415 as an example, the highest $C_L/C_D = 151.84$ is observed at an angle of attack of $\alpha = 5^0$. When the Reynolds number increases to $Re = 4 \times 10^6$, the maximum lift-to-drag ratio is $C_L/C_D = 171.48$ for the NACA 4415 airfoil, which is marked in Fig. 5b. In the case of NACA 23012 and NACA 23015 airfoils, they have smaller lift-to-drag ratios for the targeted range of Reynolds numbers $2E6 \leq Re \leq 1E7$. Additionally, the lift-to-drag ratio of the four NACA is compared by considering the Reynolds number $Re = 6 \times 10^6$ at an angle of attack $\alpha = 9^0$ as shown in Fig. 5c.The highest $C_L/C_D = 146.09$ and the lowest $C_L/C_D = 138.62$ are obtained on NACA 23015 and NACA 4415 airfoils. As the Reynolds numbers increased to $Re = 8 \times 10^6$ and $Re = 1 \times 10^7$, the difference in lift-to-drag ratios increased to 7.16% and 12.94%, respectively. The theoretical results show that the maximum lift-to-drag ratio of each airfoil is dependent on the Reynolds numbers and angles of attack. It is necessary to set the maximum lift-to-drag ratio as the optimal target in order to improve the power coefficient.

Here, the lift-to-drag ratio at the Reynolds number of $Re = 6 \times 10^6$ and the new design angle of attack of$\alpha_D = 9^0$ are considered to determine the chord length of each airfoil and to position the airfoils along the length of the 54 m HAWT blade. The values of lift coefficient, drag coefficient, and lift-to-drag ratio used to model the chord length for the proposed HAWT are shown in Table 3. Results show that the lift-to-drag ratio of the NACA 4420 airfoil has the lowest and the NACA 23015 airfoil has the highest value. This difference comes due to the lower drag coefficient of the NCAC 23015 airfoil. To maximize the power output of a rotor, airfoils with a higher lift-to-drag ratio and lower drag coefficients must be placed on the tip section of the blade.

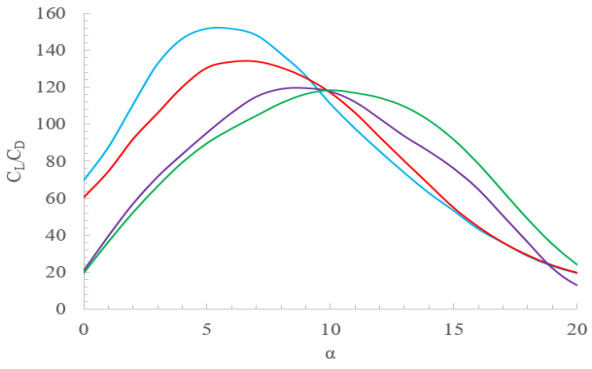

(a)

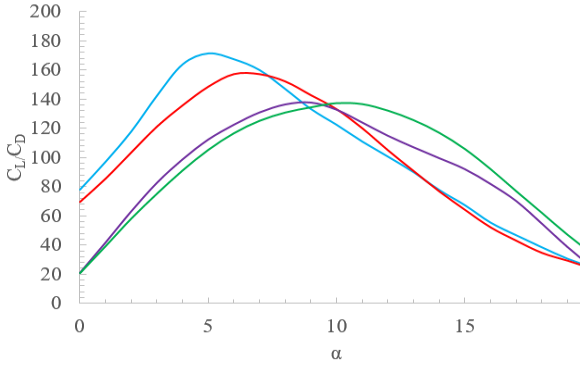

(b)

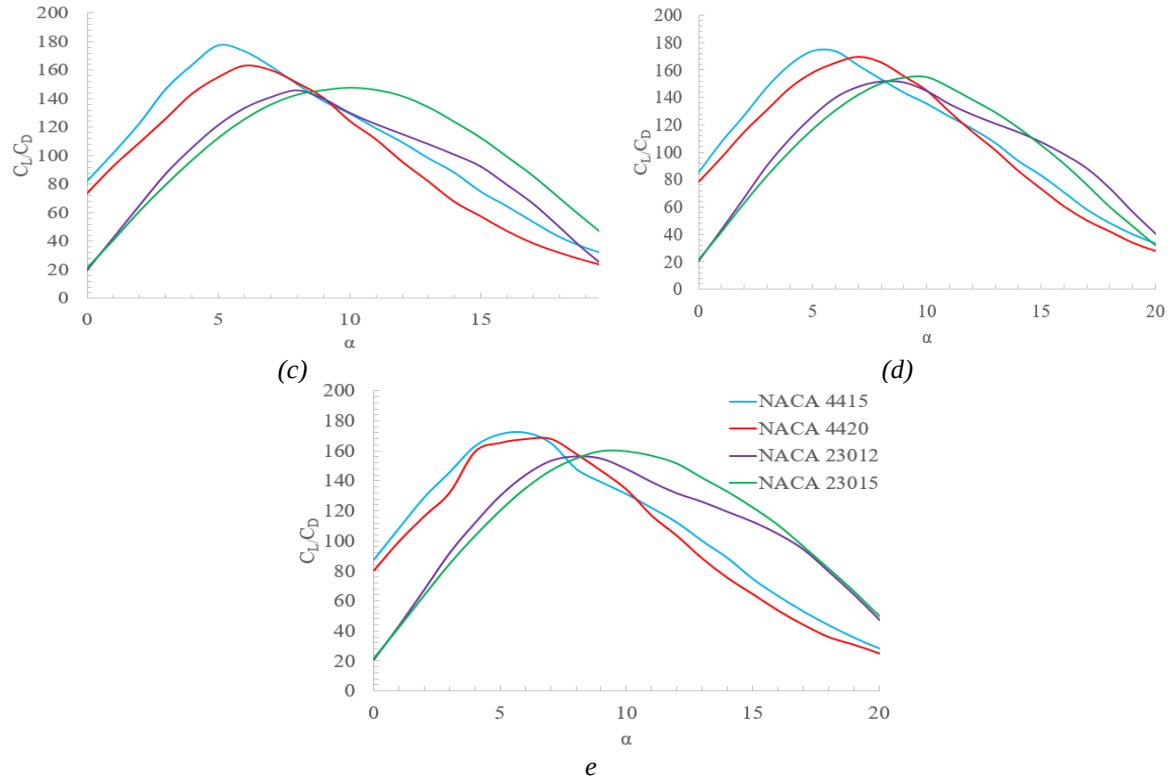

Figure 5. Lift-to-drag ratios of airfoils at different angles of attack and different Reynolds numbers, (a) $Re = 2 \times 10^6$, (b) $Re = 4 \times 10^6$, (c) $Re = 6 \times 10^6$, (d) $Re = 8 \times 10^6$, and (e) $Re = 1 \times 10^7$.

Table 3. Drag coefficient and the lift-to-drag ratio at $Re = 6 \times 10^6$ and at a design angle of attack $\alpha_D = 9^0$.

Airfoils	NACA 4415			NACA 4420			NACA 23012			NACA 23015		
Parameter	Cd	Cl	Cl/Cd	Cd	Cl	Cl/Cd	Cd	Cl	Cl/Cd	Cd	Cl	Cl/Cd
Re: 6E6	0.010	1.431	138.62	0.009	1.409	151.35	0.008	1.155	145.77	0.008	1.138	146.09

4.2. CFD Simulation Results

CFD is one method to assess the aerodynamic performance of an airfoil that is similar to a wind tunnel test. The cost and time needed to determine the airfoil's performance are lower than those of the wind tunnel test. In this study, ANSYS Fluent software was executed to predicate the performance of the airfoils to set their optimal position along the length of a 54 m wind turbine blade. To ensure the accuracy of the results, three different mesh sizes were considered, corresponding to 40 K, 89 K, and 246 K elements, respectively. The computed results are compared within each airfoil family, as shown in Table 4. The simulation results indicate that the NACA 23012 airfoil has the highest velocity magnitude and the lowest static pressure for 40 K and 89 K mesh elements. However, the highest velocity magnitude was obtained for the NACA 23015 airfoil at 246 K. The turbulence kinetic energy of the airfoil increased as the wind speed increased at the targeted mesh sizes. Based on the CFD simulation results, the NACA 23012 airfoil has better aerodynamic performance than other airfoils. It is a good candidate to be set at the tip section of the newly designed 54 m wind turbine blade.

Table 4. Turbulence kinetic energy, velocity magnitude and pressure distribution for each airfoil at different wind speeds and mesh numbers.

Wind speed (m/s)	Mesh numbers	Airfoil types	Velocity magnitude (m/s)	Static pressure (Pascal)	Turbulence kinetic (m^2/s^2)
6	40000	NACA 23015	9.09	21.60	1.88
		NACA 23012	9.40	21.20	0.88
		NACA 4420	8.83	21.70	1.38
		NACA 4415	9.20	21.40	0.78
9		NACA 23015	13.70	48.50	4.21
		NACA 23012	14.20	47.40	1.98
		NACA 4420	13.30	48.50	2.96

		NACA 4415	14.00	48.10	1.63
12		NACA 23015	18.30	86.20	7.45
		NACA 23012	18.90	84.30	3.42
		NACA 4420	17.80	86.20	5.11
		NACA 4415	18.70	85.50	2.75
6	89000	NACA 23015	9.38	21.80	1.15
		NACA 23012	9.52	21.60	0.87
		NACA 4420	9.04	21.80	1.29
		NACA 4415	9.27	21.70	1.00
9		NACA 23015	14.10	48.90	2.58
		NACA 23012	14.30	48.50	1.88
		NACA 4420	13.60	49.10	2.74
		NACA 4415	14.00	48.90	1.87
12		NACA 23015	18.90	87.00	4.56
		NACA 23012	19.20	86.00	3.28
		NACA 4420	18.30	87.30	4.68
		NACA 4415	18.70	86.90	2.99
6	246000	NACA 23015	9.64	21.90	1.05
		NACA 23012	9.60	21.80	1.17
		NACA 4420	9.13	21.90	1.22
		NACA 4415	9.28	21.80	1.20
9		NACA 23015	14.60	49.30	2.21
		NACA 23012	14.40	49.00	2.09
		NACA 4420	13.80	49.30	2.54
		NACA 4415	14.00	49.10	2.33
12		NACA 23015	19.50	87.60	3.72
		NACA 23012	19.30	87.10	3.45
		NACA 4420	18.60	87.60	4.00
		NACA 4415	18.80	87.40	3.84

The static pressure and velocity contour of the four airfoils at a wind speed of 12 m/s and an AOA$\alpha_D = 9^0$ were compared as shown in Figs. 6 and 7. The simulation results show similarities in static pressure between the four and five-digit airfoils. However, the velocity magnitude of the airfoils was varied, and a better velocity magnitude was obtained for the case of five-digit airfoils.

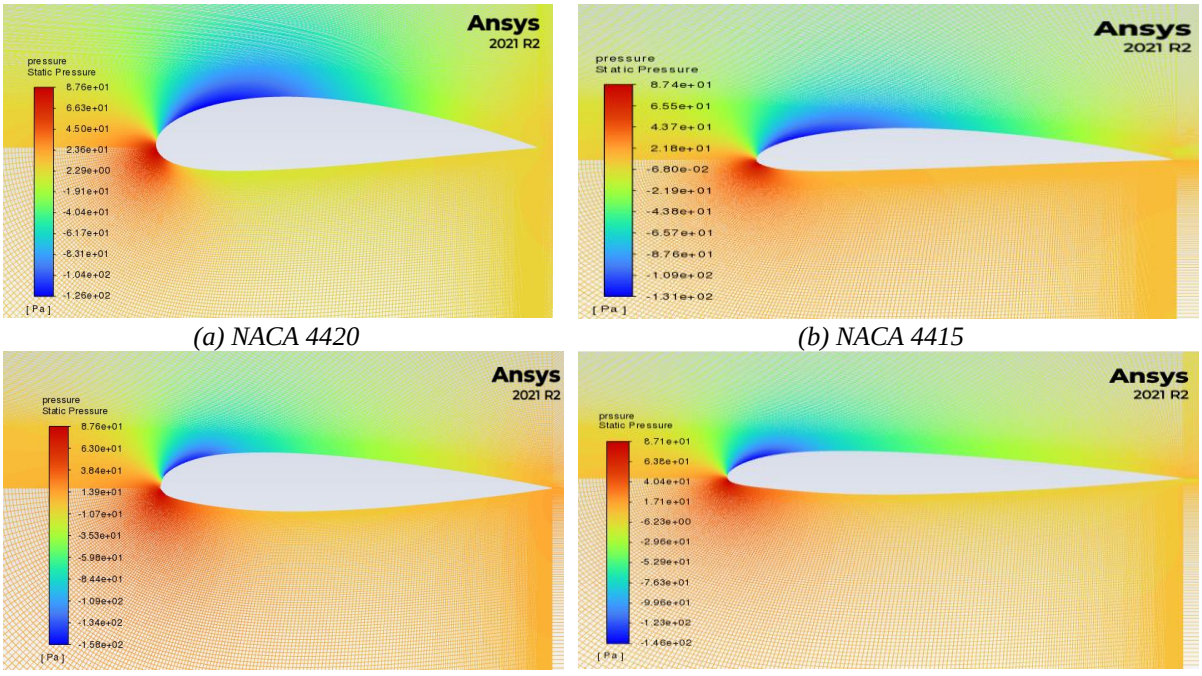

(a) NACA 4420 *(b) NACA 4415*

(c) NACA 23015 *(d) NACA 23012*

Figure 6. Static pressure contour of NACA23015, NACA 23012, NACA 4420 and NACA 4415 airfoils at a wind speed of 12 m/s and $\alpha_D = 9^0$.

As shown in Fig. 7 (a), the velocity magnitude of NACA 23015 is the highest and NACA 4420 is the lowest. This shows different airfoils are needed to model a blade along its length to extract the maximum energy from the wind. The thickness of the airfoils is an additional parameter to decide the position of the airfoil. In particular, thick airfoils are needed for the root section of the blade for the stability of the blade structure. However, the NACA 23015 airfoil has a higher thickness compared to the NACA 23012 airfoil. In this case, placing NACA 23012 (thinner thickness) at the blade's tip section can improve the power coefficient better than the other airfoils.

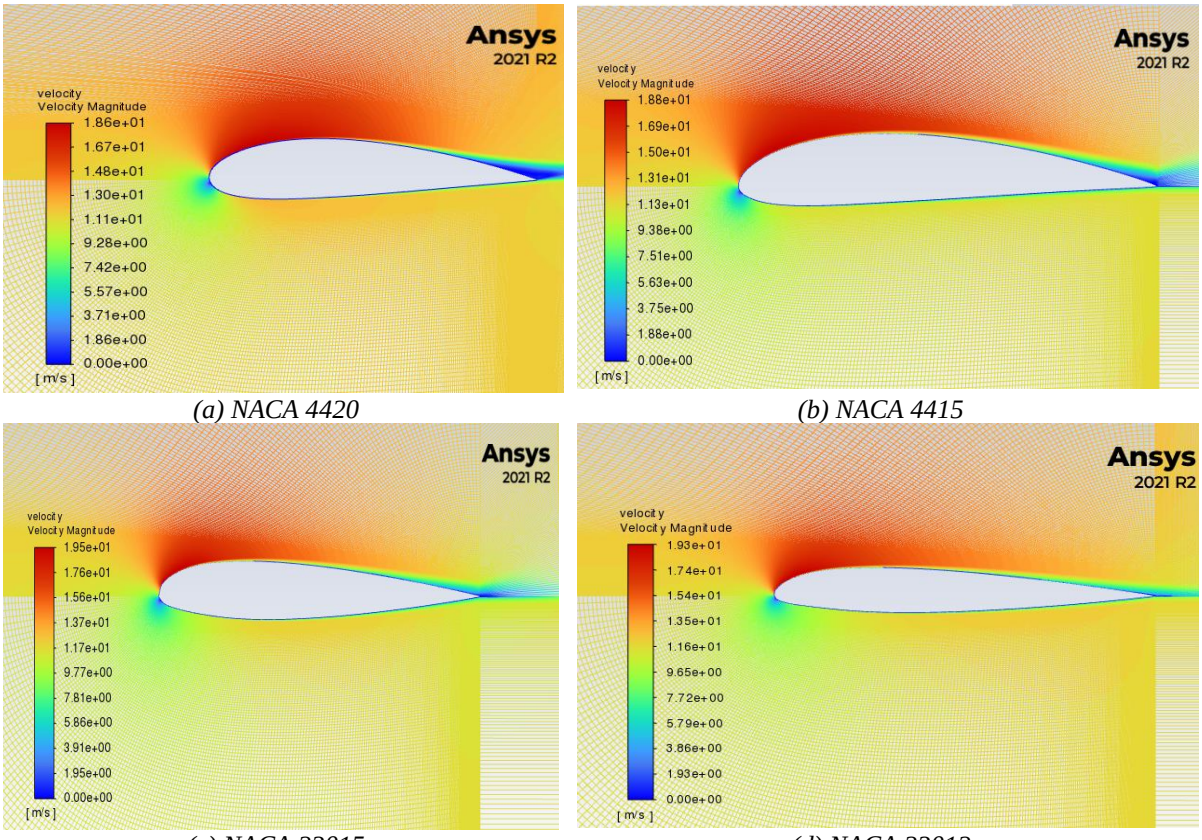

(a) NACA 4420 *(b) NACA 4415*

(c) NACA 23015 *(d) NACA 23012*

Figure 7. Velocity magnitude contour of NACA23015, NACA 23012, NACA 4420 and NACA 4415 airfoils at a wind speed of 12 m/s and $\alpha_D = 9^0$.

4.3 Numerical Results

BEMT is the most popular technique to determine the design parameters of wind turbine blades, such as section twist angles, flow angles, induction factors, and chord lengths of the rotor. The model divides the blade into small elements and operates the aerodynamic performance as 2D airfoils whose design parameters can be calculated based on local flow conditions [15]. In this study, BEMT was used to find and characterize the chord length and flow angles of NACA 4420, NACA 4415, NACA 23015, and NACA 23012 airfoils under TSR of 7, 8, and 9 to model a 54 m HAWT blade using each airfoil. Tables 5 and 6 show the values of optimized chord length and the flow angle along the length of the twelve blades at TSR of 7, 8, and 9 after many iterations. Results indicate that the chord lengths and flow angles decreased as the TSR increased. In addition, the chord length and flow angle properties of each airfoil under the specified TSR were examined. The values of chord length and flow angle significantly increased towards the root section. TSR is an important parameter in blade design to ensure satisfactory performance [35]. It is important to understand that linearization techniques at various TSRs can optimize the aerodynamic performance of the blade. In this case, the highest and the lowest chord length are observed for NACA 23015 airfoil and NACA 4420 airfoil at each specified TSR after linearization. The aerodynamic performance of the rotor depends on the size of the chord length of the airfoils. As the size of the blade increases, the aerodynamic performance may be reduced at lower wind speeds. On the

other hand, lower TSR corresponds to high wind conditions. Due to this, it is necessary to develop the HAWT blades by using different airfoil families to obtain an optimized chord length that can maximize the aerodynamic performance. Moreover, the section twist distributions under TSR of 7, 8, and 9 are assessed on the four and five-digit NACA airfoils as shown in Fig. 8. The results show that the sectional twist distributions of the airfoils decreased as the TSR increased.

Table 5. Geometric dimensions of rotor blades having four-digit NACA 4415 and NACA 4420 airfoils.

	NACA 4415						NACA 4420					
	TSR 7		TSR 8		TSR 9		TSR 7		TSR 8		TSR 9	
	$c(r)$	φ	$c(r)$	φ	$c(r)$	φ	$c(r)$	φ	c(r)	φ	$c(r)$	φ
r/R	meter	degree	meter	degree	meter	degree	meter	degree	meter	degree	meter	degree
0.20	6.48	25.51	5.07	22.66	4.07	20.35	6.58	25.51	5.15	22.66	4.14	20.35
0.29	4.72	18.27	3.66	16.11	2.91	14.40	4.79	18.27	3.71	16.11	2.96	14.40
0.38	3.68	14.16	2.84	12.45	2.25	11.10	3.74	14.16	2.88	12.45	2.29	11.10
0.47	3.01	11.55	2.32	10.14	1.84	9.03	3.06	11.54	2.35	10.13	1.87	9.03
0.56	2.55	9.74	1.95	8.54	1.55	7.60	2.59	9.73	1.99	8.54	1.57	7.60
0.64	2.20	8.41	1.69	7.38	1.34	6.56	2.24	8.41	1.72	7.37	1.36	6.56
0.73	1.94	7.41	1.49	6.48	1.18	5.77	1.97	7.40	1.51	6.49	1.20	5.77
0.82	1.73	6.61	1.33	5.79	1.05	5.15	1.76	6.61	1.35	5.79	1.07	5.15
0.91	1.57	5.97	1.20	5.23	0.95	4.65	1.59	5.97	1.22	5.23	0.96	4.65
1.00	1.43	5.44	1.09	4.77	0.87	4.24	1.45	5.44	1.11	4.77	0.88	4.24

Table 6. Geometric dimensions of rotor blades having five-digit NACA 23012 and NACA 23015 airfoils.

	NACA 23012						NACA 23015					
	TSR 7		TSR 8		TSR 9		TSR 7		TSR 8		TSR 9	
	$c(r)$	φ	$c(r)$	φ	$c(r)$	φ	$c(r)$	φ	$c(r)$	φ	$c(r)$	φ
r/R	meter	degree	meter	degree	meter	degree	meter	degree	meter	degree	meter	degree
0.20	8.03	25.51	6.29	22.66	5.04	20.35	8.15	25.51	6.38	22.66	5.12	20.35
0.29	5.85	18.27	4.53	16.11	3.60	14.40	5.93	18.27	4.60	16.11	3.66	14.40
0.38	4.56	14.16	3.52	12.45	2.79	11.10	4.63	14.16	3.57	12.45	2.84	11.10
0.47	3.73	11.55	2.87	10.13	2.28	9.03	3.79	11.54	2.91	10.13	2.31	9.03
0.56	3.15	9.73	2.42	8.54	1.92	7.60	3.20	9.73	2.46	8.54	1.95	7.60
0.64	2.73	8.41	2.09	7.37	1.66	6.56	2.77	8.41	2.13	7.37	1.68	6.56
0.73	2.40	7.40	1.84	6.49	1.46	5.77	2.44	7.40	1.87	6.49	1.48	5.77
0.82	2.15	6.61	1.65	5.79	1.30	5.15	2.18	6.61	1.67	5.79	1.32	5.15
0.91	1.94	5.97	1.49	5.23	1.18	4.65	1.97	5.97	1.51	5.23	1.19	4.65
1.00	1.77	5.44	1.34	4.77	1.07	4.23	1.80	5.44	1.38	4.77	1.09	4.24

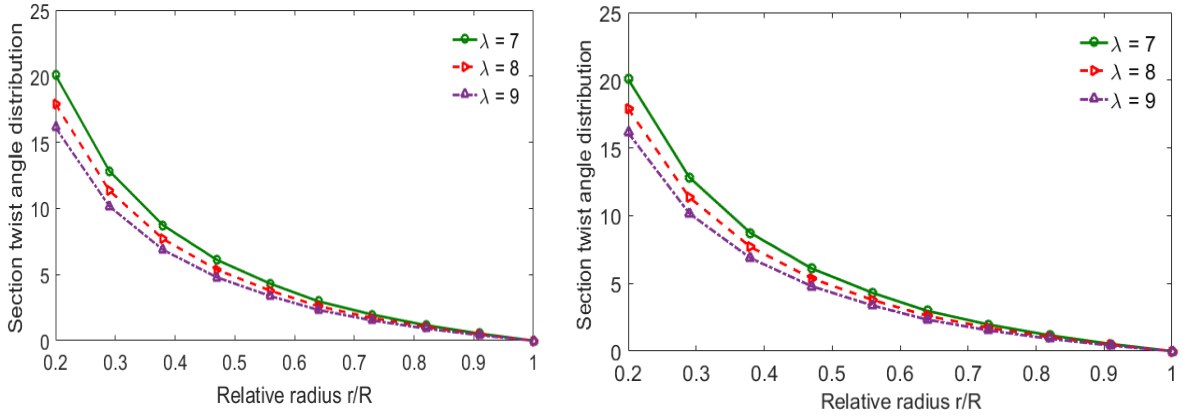

Figure 8. Twist distribution (a) NACA 4420, NACA 4415 and (b) NACA 23015, NACA 23012 airfoils.

Optimized chord lengths are required when designing a HAWT blade to reduce cost, stall, weight, and increase structural stability. As the size of the wind turbine blade increases, the load increases drastically around the root section of the blade. The greater bending loads are sustained near the root of the blade. It needs to use thick airfoils to support the large bending loads. However, thick airfoils have poor aerodynamic performance when compared to thin airfoils [36]. A key problem is to design a strong

region near the root section that supports these loads without sacrificing too much aerodynamic performance. For comparison, a 54 m HAWT blade was developed using NACA airfoil families. Each of the NACA 4420, NACA 23015, NACA 4415, and NACA 23012 airfoils were applied to develop the wind turbine blades at TSR of 7, 8, and 9. The distribution of NACA airfoils along the length of 54 m HAWT was performed using optimized thickness distribution techniques. Figs. 9 and 10 show the thickness distribution on the HAWT blades that were developed using four and five-digit NACA airfoils at TSR of 7, 8 and 9. The highest and the lowest thickness distribution were observed on the blades that were developed by using the NACA 4420 airfoil and the NACA 23012 airfoil on each specified TSR. In this case, the wind turbine blades developed by using NACA 4420 can be good for structural stability. On the other hand, wind turbine blades developed using NACA 23012 can have good aerodynamic performance. The aerodynamic and structural properties of the airfoils are important in blade design. It is necessary to consider these parameters during the design of the blade. Mainly, the stresses reach their maximum and minimum values around the root and the tip of the blade. To overcome these stresses, thicker and thinner airfoils at each section are needed. A thicker airfoil (NACA 4420) was set around the root section and a thinner airfoil (NACA 23012) was set at the tip section for the newly designed 54 m wind turbine blade. Based on thickness distribution techniques of the airfoils, NACA 4420, NACA 23015, NACA 4415, and NACA 23012 airfoils were set at 20%, 37.78%, 55.56%, and 91.11% of the full length of the blade. The remaining sections of the blades were set based on linear interpolation techniques by estimating values considering the two extreme positions. Both chord lengths and thickness distributions are optimized using this technique. In particular, the maximum chord length of the newly designed rotor blade was reduced by 18.06% compared to the NACA 23012 rotor blade.

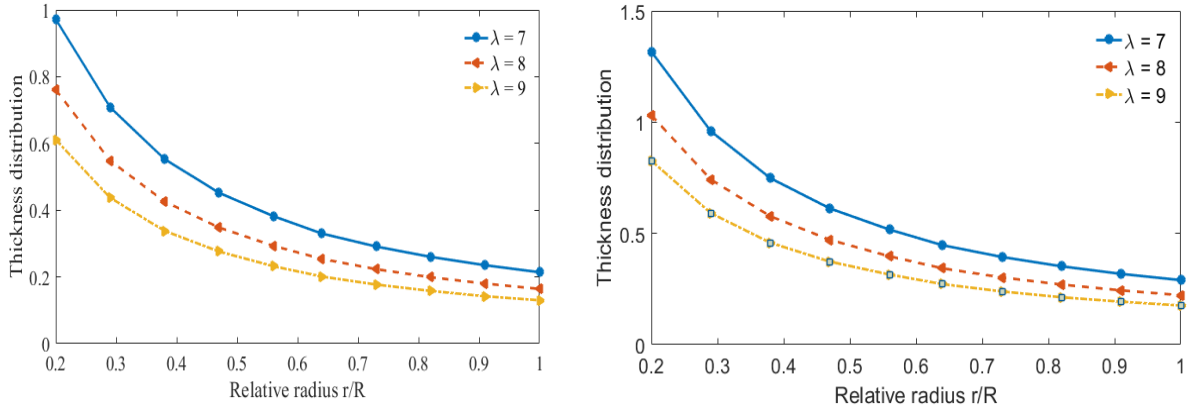

(a) *(b)*

Figure 9. Thickness distribution for four-digit (a) NACA 4415, and (b) NACA 4420 airfoils.

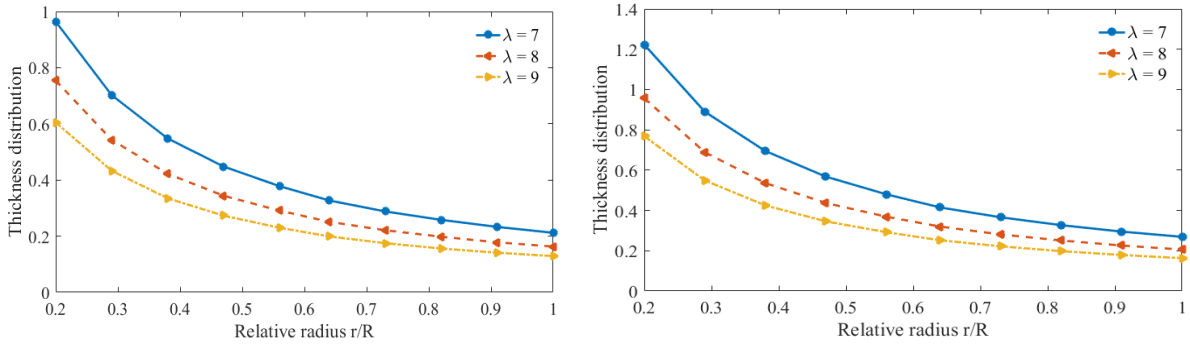

(a) *(b)*

Figure 9. Thickness distribution for five-digit (a) NACA 23012, and (b) NACA 23015 airfoils.

Based on BEMT, the normal and tangential forces on the newly designed 54 m HAWT blades are analyzed under different TSR and wind speeds. As shown in Fig. 11, the normal and tangential forces

increased towards the tip section of the blades as the wind speeds increased. In addition, the relative wind velocity increased towards the tips of the blades due to the reduction in the flow angle. A blade which is designed for high relative wind speeds develops minimal torque at lower speeds [37]. Mostly, tangential forces are used to generate torque. Additionally, the normal and tangential forces on the newly designed blade are characterized as a function of TSR of 7, 8, and 9 as shown in Figs. 11 (a-c). The graphical results show nearly similar normal and tangential forces on each targeted TSR and wind speed. However, the normal and tangential forces increased as the wind speed changed from 6 to 12 m/s. A higher tip speed demands reduced chord length, leading to narrow blade profiles. This can lead to reduced material usage and lower production costs. Although an increase in centrifugal and aerodynamic forces is associated with higher tip speeds. The chord length of the newly designed blade was compared as a function of TSR. As the TSR increased from 7 to 9, the chord length was reduced by about 37.19%. It is observed that reducing the chord length has a direct effect on reducing the weight and the cost of the wind turbine. Based on the current numerical results, TSR at 9 is recommended for the design of large hybrid HAWTs from weight and cost viewpoints.

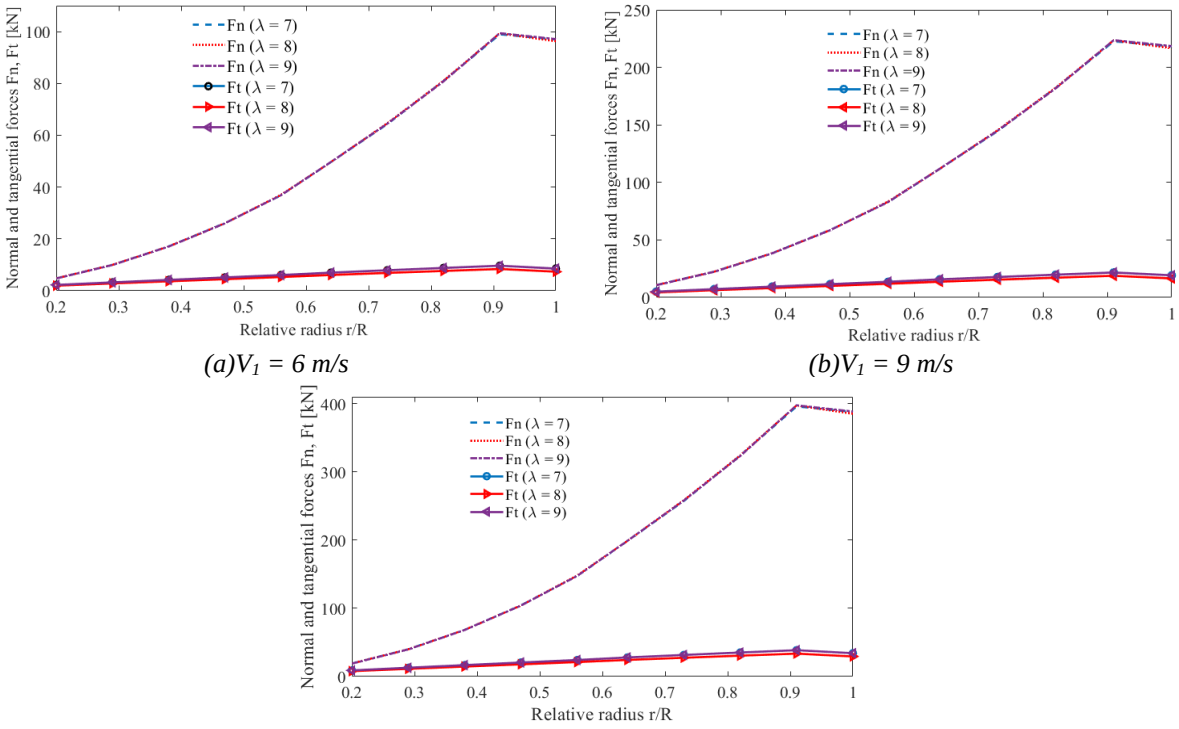

(a)V_1 = 6 m/s *(b)V_1 = 9 m/s*

(c) V1 = 12 m/s

Figure 10. Force distributions on hybrid HAWTs at different TSR and wind speeds.

5. CONCLUSIONS

This study is part of ongoing research to assess the performance of different airfoils to design the structure of wind turbine blades applicable to different wind farms. The purpose of this paper is to determine the best position of the airfoil along the length of the proposed 54 m horizontal axis wind turbine blades. The highest lift coefficient and the lift-to-drag ratio of airfoils at AOA ($\alpha_D = 9^0$) and Reynolds numbers ($Re = 6 \times 10^6$) were considered for four-digit (NACA 4415 and NACA 4420) and five-digit (NACA 23012 and NACA 23015) airfoils. The aerodynamic parameters of the airfoils are obtained using Qblade/Xfoil open software. BEM theory was used to assess the power coefficient, chord length, induction factors, and twist distribution of airfoils. All the parametric values were optimized using MATLAB codes. Results from the theoretical investigation indicated that chord length, induction factors, twist and thickness distributions of each airfoil were varied. Mostly, higher stresses around the root and lower stresses at the tip sections were observed in the rotor blades. Additionally, variations in

chord length between four and five-digit airfoils were observed. Based on thickness distribution techniques of airfoils, NACA 4420, NACA 23015, NACA 4415, and NACA 23012 airfoils were set at 20%, 37.78%, 55.56%, and 91.11% of the full length. The remaining portion of the region between the root and the maximum chord was covered with a circular profile. The normal and tangential forces acting on the newly developed HAWTs were analyzed using different TSRs. The TSRs were observed to be nearly similar for each force. Based on this, a higher tip speed ratio, which is 9, is recommended for the design of a hybrid HAWT.

Acknowledgement

The research reported in this paper was supported by the University of KwaZulu-Natal (UKZN), National Research Foundation of South Africa (NRF) and DDU. The authors gratefully acknowledge the support provided by UKZN, NRF and DDU.

REFERENCES

[1] Saenz-Aguirre, A, Fernandez-Gamiz, U, Zulueta, E, Ulazia, A, Martinez-Rico, J. Optimal wind turbine operation by artificial neural network-based active gurney flap flow Control. *Sustainability* 2019; *11*: 2809. DOI: 10.3390/su11102809.
[2] Joyce, L, Feng, Z. Global wind report. Brussels, Belgium: Global Wind Energy Council, 2022.
[3] Fernandez-Gauna, B, Fernandez-Gamiz, U, Graña, M. Variable speed wind turbine controller adaptation by reinforcement learning. *Integrated Computer-Aided Engineering* 2017; *24*: 27–39. DOI: 10.3233/ICA-160531.
[4] Ezio, S, Norman, L. Wind energy in Europe. Wind Engineering 1992; *16*: 35–47.
[5] Hamed, S, Pooria, A, Ali, S. Aerodynamic performance enhancement of horizontal axis wind turbines by dimples on blades: Numerical investigation. *Energy* 2020; *195*: 117056. DOI: 10.1016/j.energy.2020.117056.
[6] Eleni, D, Dionissios, M. Aerodynamic performance investigation under the influence of heavy rain of a NACA 0012 airfoil for wind turbine applications. *International Review of Mechanical Engineering* 2012; *6*: 1228–1235. DOI:10.15866/ireme.v6i6.20761.
[7] Bili, S, Gaguk, J, Muh, K. Characteristic analysis of horizontal axis wind turbine using airfoil NACA 4712. *Journal of Mechanical Engineering Science and Technology* 2019; *3*: 96–108. DOI: 10.17977/um016v3i22019p096.
[8] Jureczko, M, Pawlak, M, Mężyk, A. Optimisation of wind turbine blades. *Journal of Material Processing Technology* 2005: *167*: 463–471. DOI: 10.1016/j.jmatprotec.2005.06.055.
[9] Ernesto, B, Andrea, T. Optimal design of horizontal-axis wind turbines using blade-element theory and evolutionary computation. *Journal of Solar Energy Engineering* 2002: *124*: 357–363. DOI: 10.1115/1.1510868.
[10] Thang, Le-Duc, Quoc-Hung, N. Aerodynamic optimal design for horizontal axis wind turbine airfoil using integrated optimization method. *International Journal of Computational Methods* 2019; *16*: 1–15. DOI: 10.1142/S0219876218410049.
[11] Sang-Lae, L, Sang, S. Structural design optimization of a wind turbine blade using the genetic algorithm. *Engineering Optimization* 2021. DOI: 10.1080/0305215X.2021.1973450.
[12] Grasso, F. Usage of numerical optimization in wind turbine airfoil design. *Journal of Aircraft* 2011; *48*: 248–255, DOI: 10.2514/1.C031089.
[13] Chaudhary, K, Roy, A. Design and optimization of a small wind turbine blade for operation at low wind speed. *World Journal of Engineering* 2015; *12*: 83–94. DOI: 10.1260/1708-5284.12.1.83.
[14] Haci, S, Ismail, B. Calculation of optimum angle of attack to determine maximum lift to drag ratio of NACA 632-215 airfoil. *Journal of Multidisciplinary Engineering Science and Technology* 2015; *2*: 1103–1108.
[15] Mehmet, B, Sezayi, Y. Theoretical and computational investigations of the optimal tip-speed ratio of horizontal-axis wind turbines. *Engineering Science and Technology, an International Journal* 2018; *21*: 1128–1142. DOI: 10.1016/j.jestch.2018.05.006.
[16] Ribeiro, A. F. P, Awruch, A. M, Gomes, H. M. An airfoil optimization technique for wind turbines. *Applied Mathematical Modelling* 2012; *36*: 4898–4907. DOI: 10.1016/j.apm.2011.12.026.
[17] Yang, Y, Chun, L, Wanfu, Z, Jun, Y, Zhou, Y, Weipao, M, Kehua, Y. A multi-objective optimization for HAWT blades design by considering structural strength. *Journal of Mechanical Science and. Technology* 2016; *30*: 3693–3703, DOI: 10.1007/s12206-016-0731-3.

[18] Jerson Rogério Pinheiro,V, João Tavares, P, André Luiz Amarante, M. An extension of BEM method applied to horizontal-axis wind turbine design. *Renewable Energy* 2011; *36*: 1734–1740. DOI: 10.1016/j.renene.2010.11.018.
[19] Hua, Y, Wen, S, Haoran, X, Zedong, H, Chao, L. Prediction of the wind turbine performance by using BEM with airfoil data extracted from CFD. *Renewable Energy* 2014; *70*: 107–115. DOI: 10.1016/j.renene.2014.05.002.
[20] Tenguria, N, Mittal, N, Ahmed, S. Investigation of blade performance of horizontal axis wind turbine based on blade element momentum theory (BEMT) using NACA airfoils. *International Journal of Engineering, Science and Technology* 2010; *2*: 25–35. DOI: 10.4314/ijest.v2i12.64565.
[21] Jie, Z, Xin, C, Pan, P, Rongrong, G. Multi-objective structural optimization design of horizontal-axis wind turbine blades using the non-dominated sorting genetic algorithm II and finite element method. *Energies* 2014; *7*: 988–1002. DOI: 10.3390/en7020988.
[22] Muhammad, M, Abdur, R, Muhammad, I, Mustansar, S, Noor, R. Design optimization and analysis of rotor blade for horizontal-axis wind turbine using Q-Blade software. *Pakistan Journal of Science and Industrial Research Series A Physical Sciences* 2021; *64*: 65–75.
[23] Padmanabhan, K, Saravanan, R. Study of the performance and robustness of NREL and NACA 2D blade profiles for wind turbine applications. *European Journal of Scientific Research* 2012; *11*: 59–72.
[24] Bhadake, P. G, Gore, V. G. A Review on Aerodynamic Analysis of Horizontal Axis Wind Turbine Blade Using CFD Technique. *International Journal of Engineering and Applied Sciences* 2016; *3*: 16–18.
[25] Mulugeta, A, Gerawork, A. Aerodynamic design of horizontal axis wind turbine blades. *FME Transactions* 2017; *45*: 647–660. DOI: 10.5937/fmet1704647M.
[26] Han, C. Aerodynamics analysis of small horizontal axis wind turbine blades by using 2D and 3D CFD modelling. MSc, University of Central Lancashire, Preston, England, 2011.
[27] Carlo C. CFD-RANS study of horizontal axis wind turbines. PhD, University of Cagliari, Cagliari, Italy, 2008.
[28] Mingwei, G, De, T, Ying, D. Reynolds number effect on the optimization of a wind turbine blade for maximum aerodynamic efficiency. *Journal Energy Engineering* 2016; *142*: 04014056. DOI: 10.1061/(asce)ey.1943-7897.0000254.
[29] Getahun T. Design and testing of a composite material for modelling wind turbine blade structures in a tropical region. PhD, University of KwaZulu-Natal, Durban, South Africa, 2018.
[30] Manwell, J. F, McGowan, J. G. Wind energy explained theory, design and application. West Sussex, United Kingdom: A John Wiley and Sons Ltd Publication, 2009.
[31] Morgado, J, Vizinho, R, Silvestre, R, Páscoa, C. XFOIL vs CFD performance predictions for high lift low Reynolds number airfoils. *Aerospace Science and Technology* 2016; *52*: 207–214. DOI: 10.1016/j.ast.2016.02.031.
[32] Mustafa, Y, Hasan, K, Erkan, Ç, Ziya, C. A comparative CFD analysis of NACA0012 and NACA4412 airfoils. J*ournal of Energy System* 2018; *2*: 145–159. DOI: 10.30521/jes.454193.
[33] Mostafa, F, Mahdi, A, Omid, N, Ali, M, Kyung, K. Aerodynamic performance improvement of wind turbine blade by cavity shape optimization. *Renewable Energy* 2019; *132*: 773–785. DOI: 10.1016/j.renene.2018.08.047.
[34] Zhou, T, Cao, H, Zhang, M, Liao, C. Performance simulation of wind turbine with optimal designed trailing-edge serrations. *Energy* 2022; *243*: 122998. DOI: 10.1016/j.energy.2021.122998.
[35] Yang, K. Geometry design optimization of a wind turbine blade considering effects on aerodynamic performance by linearization. *Energies* 2020; *13*: 2320. DOI: 10.3390/en13092320.
[36] Akay, B, Ragni, D, Ferreira, S, Van Bussel, W. Experimental investigation of the root flow in a horizontal axis wind turbine. *Wind Energy* 2014; *17*: 1093–1109. DOI: 10.1002/we.1620.
[37] Peter, S, Richard, C. Wind turbine blade design. *Energies* 2012; *5*: 3425–3449. DOI: 10.3390/en5093425.